668 | https://doi.org/10.3311/PPci.41849
Creative Commons Attribution

Periodica Polytechnica Civil Engineering, 70(2), pp. 668–683, 2026

Experimental Study on Shear Behavior of UHPC-NC Composite Members with Varying Thicknesses: Comparison with Conventional RC Beams

Hu Xu[1], Xianlei Hu[1], Jiaxu Wu[2], Qingliang Zhan[1*]

[1] College of Transportation Engineering, Dalian Maritime University, Dalian, 116026, China
[2] Hebei Expressway Group Co., Ltd. Jingqin Branch, Qinhuangdao 066000, China
[*] Corresponding author, e-mail: zhanqingliang@163.com

Received: 06 August 2025, Accepted: 21 May 2026, Published online: 17 June 2026

Abstract

This study innovatively investigates the shear behavior of UHPC-NC composite members by systematically varying key parameters—UHPC interface configuration (ribbed form), thickness (30 mm, 40 mm, 50 mm), stirrup ratio, and shear span ratio. Static loading tests were conducted on four Ultra-High Performance Concrete Reinforced (UR) beams and identical-section Reinforced Concrete Beam (RCB) counterparts. Results reveal that UR beams exhibit 150%–200% higher cracking loads, 31%–48% greater ultimate shear capacity, and significantly enhanced stiffness and ductility compared to RCB beams. Crucially, the UHPC-NC configuration transforms the brittle shear failure mode observed in RCB beams into a ductile flexural failure mode. Furthermore, steel fibers within the UHPC synergize with stirrups to progressively resist shear deformation, effectively mitigating the widening of main cracks. A quantitative relationship between UHPC thickness and shear performance was established, providing valuable engineering design guidelines for bridge reinforcement and semi-precast construction applications. These findings demonstrate the substantial benefits of UHPC integration in enhancing the shear resistance and failure characteristics of composite structural members.

Keywords

ultra-high performance concrete (UHPC), shear behavior, composite beams

1 Introduction

With the global advancement of bridge construction technology, tens of thousands of bridges are currently in service [1–3]. Aging bridges require safe and reliable reinforcement, while new projects demand both construction efficiency and superior structural performance [4]. Conventional reinforced concrete (RC) structures, the predominant bridge form, commonly suffer from shear cracking during their service life [5, 6].

Currently, common reinforcement methods include steel plate bonding, carbon fiber reinforcement polymer (CFRP) bonding, and section enlargement [7–9]. These methods typically focus on using traditional materials and technologies to enhance and improve the mechanical properties of concrete structures. For instance, Qiang et al. [10] conducted bending performance tests on RC bridge decks reinforced with bonded steel plates. Their study found that this method offers relatively simple construction processes. However, steel plates are prone to corrosion and have poor fire resistance. Guo et al. [11] investigated the impact resistance of RC beams reinforced with CFRP. Through experiments and simulation models, they analyzed the mechanical parameters during the impact process, along with the cracking and damage conditions of the beams. Yet, compared to traditional steel reinforcements, the cost of CFRP can be relatively high [12]. Additionally, the section enlargement method is a widely used technique for reinforcing concrete structures, aimed at increasing load-bearing capacity and extending service life. However, this approach also has limitations, such as adding weight to the structure, which may impose additional loads on the original structure [13].

Ultra-High Performance Concrete (UHPC) is an innovative cementitious composite composed primarily of cement, silica fume, fly ash, quartz sand, steel fibers, superplasticizers, and other admixtures [14–16]. First introduced in 1994 [17], advanced UHPC development centers on achieving a dense particle packing structure and enhancing the matrix through steel fiber

Cite this article as: Xu, H., Hu, X., Wu, J., Zhan, Q. "Experimental Study on Shear Behavior of UHPC-NC Composite Members with Varying Thicknesses: Comparison with Conventional RC Beams", Periodica Polytechnica Civil Engineering, 70(2), pp. 668–683, 2026. https://doi.org/10.3311/PPci.41849

incorporation [18]. UHPC has witnessed rapid progress and garnered significant attention [19], demonstrating exceptional mechanical properties, toughness, and durability compared to traditional normal concrete (NC) [20]. Leveraging these superior attributes, UHPC holds extensive application potential in super high-rise buildings, long-span bridge engineering [18], and other infrastructure sectors. Its rapid development has unlocked new possibilities for innovative and high-performance bridge structure enhancement [21]. Applying UHPC to reinforce conventional concrete structures or in semi-precast construction not only boosts shear resistance and durability but also enhances construction efficiency [22]. Previous studies have demonstrated that ribbed interface configurations significantly enhance interfacial bond strength compared to smooth surfaces, thereby improving the composite action between UHPC and NC [23–25]. Therefore, a ribbed interface was adopted as the baseline configuration in this study to ensure effective load transfer between the UHPC layer and the NC core. However, for both existing structure reinforcement and semi-precast applications, the interfacial shear behavior of UHPC-NC composite members and their overall shear mechanical properties require more in-depth investigation [26].

Building on UHPC and semi-precast structure advancements, scholars have initiated research on UHPC-NC composite members for semi-precast applications [27]. Huang et al. [28] conducted comparative flexural tests showing that prefabricated UHPC formwork improves RC beam failure modes, restricts crack propagation, and significantly increases cracking load [29]. Lu et al. [30] demonstrated that prefabricated UHPC-NC composite beams exhibit superior flexural performance over conventional NC beams, while Li et al. [31] found U-shaped UHPC beam shell-NC core composites outperform fully cast-in-place frames in seismic resistance. Although existing studies have yielded rich findings on UHPC-reinforced NC beams, particularly regarding flexural performance and interfacial bond strength [32], research on their shear behavior remains relatively limited. While the flexural enhancement provided by UHPC formwork has been well documented [33, 34], systematic experimental investigations into the shear performance of UHPC-NC composite members, especially with varying UHPC thicknesses, are still insufficient. Moreover, the quantitative relationship between UHPC layer thickness and shear capacity, as well as the transformation mechanism from brittle shear failure to ductile flexural failure, has yet to be clearly established.

To address these gaps, this study presents a novel investigation into the shear behavior of UHPC-NC composite members, with a primary focus on the effect of UHPC thickness. A ribbed interface configuration was adopted for all composite specimens, while the stirrup ratio (0.314%) and shear span ratio (2.1) were kept constant as controlled variables. By testing three UR composite beams with UHPC thicknesses of 30 mm, 40 mm, and 50 mm alongside an identical-section RCB beam, this research achieves three key innovations: (1) conducting a pioneering quantitative evaluation of UHPC thickness effects on cracking load, ultimate shear capacity, and stiffness; (2) realizing comprehensive performance characterization through integrated data collection on deflection, strain fields, and failure modes to reveal how UHPC transforms brittle shear failure into ductile flexural behavior, with steel fibers synergizing with stirrups to suppress crack development; and (3) providing a preliminary quantitative assessment of the influence of UHPC thickness on shear performance, offering insights for the future development of design guidelines for concrete reinforcement and precast construction.

2 Experimental program

2.1 Specimen design

In this study, three UHPC-NC composite beams were designed to investigate the effect of UHPC thickness on shear behavior. The UHPC thickness was set as the primary variable (30 mm, 40 mm, and 50 mm), while other parameters – including the interface configuration (ribbed), stirrup diameter (8 mm), stirrup ratio (0.314%), and shear span ratio (2.1) – were kept constant to ensure comparability across specimens. Additionally, one conventional reinforced concrete beam (RCB) was included as a reference. The detailed parameters of all test beams are summarized in Table 1. A ribbed interface configuration was uniformly adopted for all UR composite beams, considering its well-recognized benefits in enhancing interfacial bond and load transfer. By keeping the interface configuration constant, the study isolates the effect of UHPC thickness as the primary variable. Subsequently, shear tests under static loading conditions were conducted on the UHPC-NC composite beams to analyze the impact of different variable parameters on their shear mechanical performance.

The ordinary RCB has dimensions of 1.8 m in length, 0.32 m in width, and 0.4 m in height. It was cast using commercial C40 concrete. The bottom tension reinforcement consists of HRB400 grade steel bars with a diameter of 22 mm, providing a tensile reinforcement ratio of

Table 1 UR beam parameters of different formwork thickness

Name	UHPC form	Thickness (mm)	Diameter of stirrup (mm)	Stirrup ratio	Beam length (m)	Shear span ratio	Cross-sectional dimensions (m)
RCB	Without UHPC	0	8	0.314%	1.8	2.1	0.32 × 0.4
UR-30-D8	Ribbed UHPC	30	8	0.314%	1.8	2.1	0.32 × 0.4
UR-40-D8	Ribbed UHPC	40	8	0.314%	1.8	2.1	0.32 × 0.4
UR-50-D8	Ribbed UHPC	50	8	0.314%	1.8	2.1	0.32 × 0.4

Note: The stirrup ratio (0.314%) and shear span ratio (2.1) were kept constant across all specimens to isolate the effect of UHPC thickness. The ribbed interface configuration was uniformly adopted for all UR beams.

2.2%. Stirrups and top compression reinforcement are made from HPB300 grade steel bars with diameters of 8 mm and 10 mm, respectively. The ends of the RCB beam are supported by simple supports. The dimensions of the RCB beam model are illustrated in Fig. 1, with all measurements provided in millimeters (mm).

First, we fabricated molds for the ordinary RCB according to the specified dimensions. The RCBs were constructed using standard construction techniques. Strain gauges were carefully installed on the reinforcing steel bars to monitor their behavior during testing. Once the strain gauges were properly positioned, the rebar cage was placed into the mold. We then poured commercial C40 concrete into the mold and allowed it to cure for 28 days under controlled conditions to ensure optimal strength development.

For the fabrication of UHPC-NC composite members, we began by creating molds based on the designed dimensions. The formwork was assembled, and bolts were securely fastened at predetermined locations to facilitate the subsequent assembly process. Next, UHPC was poured into the molds. After the UHPC had sufficiently hardened, the forms were removed, revealing the UHPC components with embedded bolts. The next step involved preparing the reinforcement for the UHPC-NC composite beams. Strain gauges were meticulously attached to the rebar cage to capture detailed data on its mechanical behavior. This instrumented rebar cage was then positioned within the precast UHPC section. Finally, commercial C40 concrete was poured around the UHPC component to complete the composite beam. This integration ensures that both materials work synergistically to enhance the overall structural performance. The entire process of fabricating the UHPC-NC composite members is illustrated in Fig. 2, providing a visual guide to each step from mold preparation to final assembly.

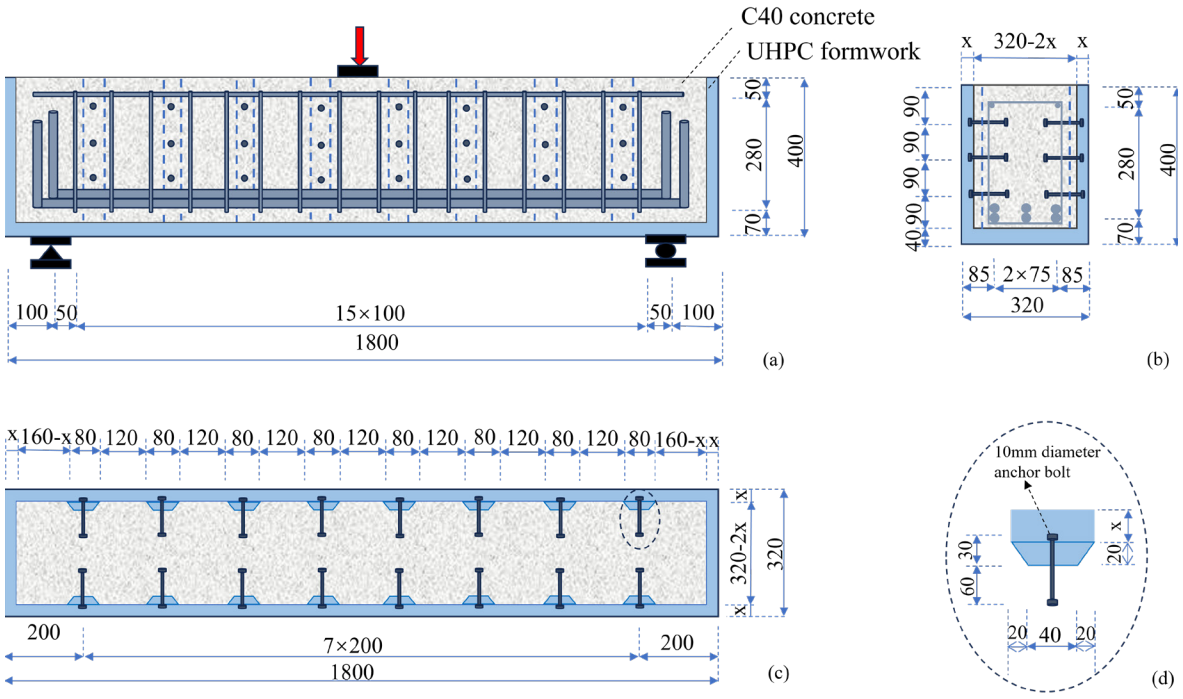

Fig. 1 UR beam structure diagram of ribbed UHPC formwork: (a) front view, (b) side view, (c) top view, and (d) enlarged view of bolt and rib dimensions

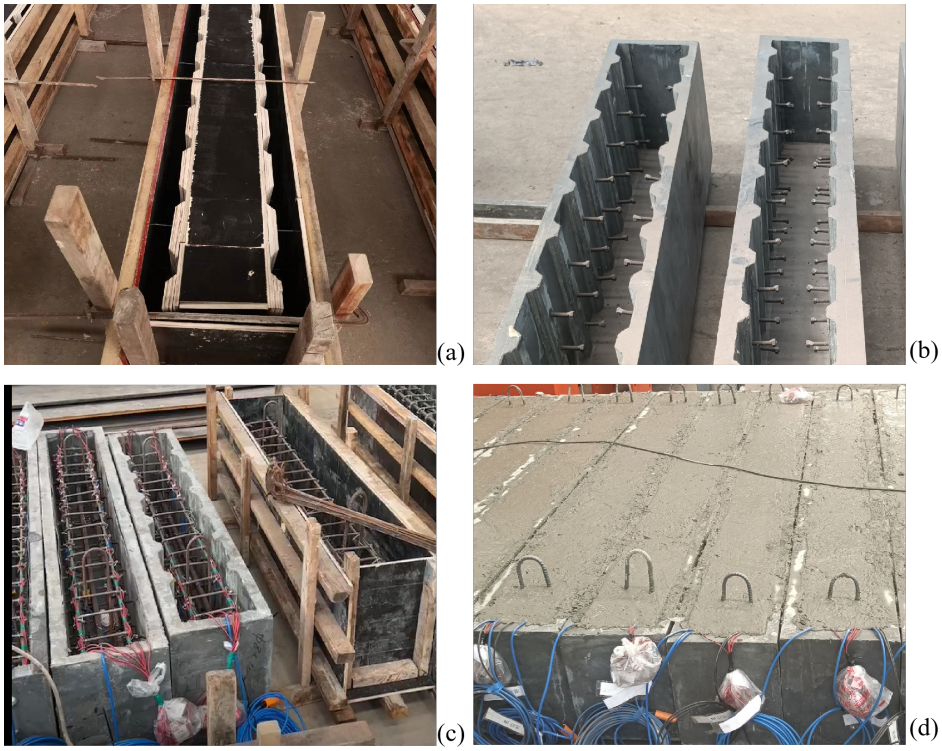

Fig. 2 Production process of UHPC-NC composite beam: (a) formwork and casting of UHPC, (b) demolding to form bolted UHPC, (c) placing the reinforcement cage and (d) UHPC-NC composite beam

2.2 Material properties of specimens

UHPC is a high-performance cementitious composite material that exhibits superior strength, toughness, and durability compared to traditional concrete. The exceptional properties of UHPC stem from its unique material composition. While conventional concrete typically uses commercial C40 concrete, the material composition and mix proportions for UHPC are detailed in Table 2. UHPC incorporates steel fibers at a volume fraction of 2.5%, specifically using copper-coated hooked-end steel fibers with a diameter of 0.2 mm and a length of 14 mm.

For the compressive strength tests, conventional concrete specimens are cubes with dimensions of 0.15 m × 0.15 m × 0.15 m, while UHPC specimens use cubes with dimensions of 0.1 m × 0.1 m × 0.1 m. The loading method for the concrete cube specimens is illustrated in Fig. 3.

Table 2 The mix ratio of UHPC

Components	Cement	Silica fume	Fly ash	Quartz sand	Water reducer	Steel fibers	Defoamer	Water
Ratio (kg/m^3)	988	96.63	191.25	1071	25.2	156	1.275	189

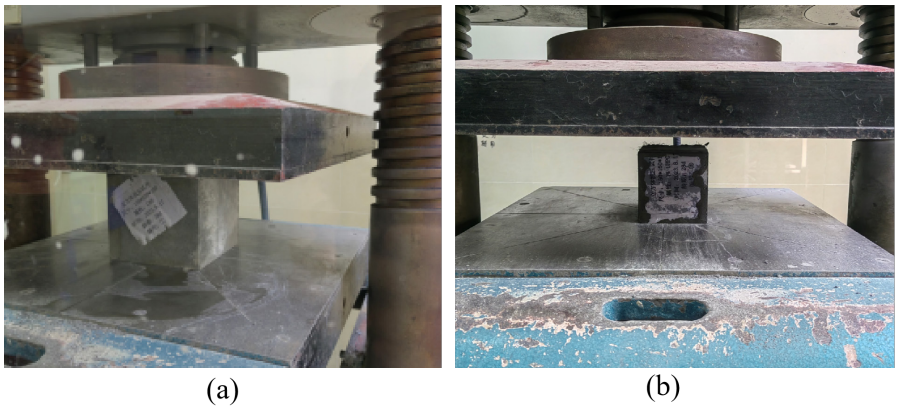

(a) (b)

Fig. 3 Concrete cube test block loading: (a) ordinary concrete (b) UHPC

The average test results are presented in Table 3.

In this study, we conducted tensile tests on reinforcing steel bars. For each type of rebar, three samples, each 50 cm in length, were retained. The mechanical properties of the rebars were obtained through these tensile tests. The setup for the rebar tensile test is illustrated in Fig. 4, and the average results of the tests are presented in Table 4.

Table 3 Performance of concrete materials

Mechanical properties	Cube compressive strength (MPa)	Elastic modulus (GPa)
Ordinary concrete (C40)	42.2	33.1
UHPC	142.3	40.9

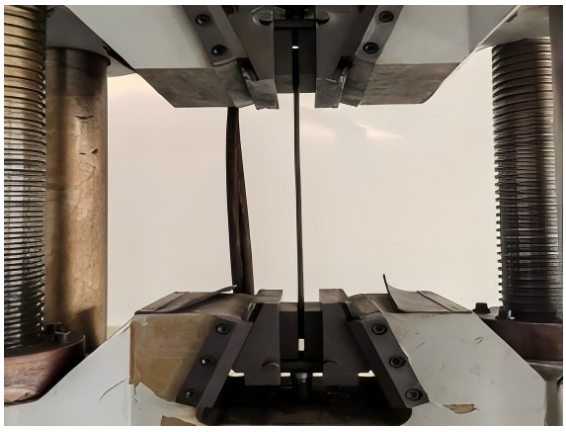

(a)

(b)

Fig. 4 Steel tensile tests: (a) 8 mm diameter HPB300 grade reinforcing bar, (b) 22 mm diameter HPB400 grade reinforcing bar

2.3 Test set-up

In this study, a 200-ton hydraulic jack was used for loading. The load is applied via the hydraulic jack and transmitted through a pressure sensor to a bearing block, which then transfers the load to the test beam. The shear performance of the model beams was evaluated using a three-point loading method. One end of the beam was horizontally constrained, while the other end was left unconstrained. To prevent stress concentration, rigid padding was employed. The loading setup is illustrated in Fig. 5.

To measure the strain in both the conventional concrete and UHPC in the compression zone, strain gauges were placed on the top surface of the beam, with their centers positioned 200 mm from the mid-span location. For analyzing the principal strain changes in the UHPC on the side of the beam, rosette strain gauges were arranged on the side surface of the beam. These rosettes consisted of strain gauges oriented at 0°, 45°, and 90° angles and were evenly distributed along the line connecting the center of the loading point to the center of the support, with a total of four rosettes installed. Additionally, to monitor the cracking load at the bottom edge of the beam, a strain gauge was placed 70 mm above the bottom surface of the beam.

For all model beams, the strain measurement points for stirrups and longitudinal reinforcement are consistently positioned. For the stirrups, strain gauges are placed starting from the center of the top longitudinal bars and extend 200 mm outward on both sides along the longitudinal direction of the beam. Additionally, strain gauges are installed every 70 mm vertically downward from the top. The analysis focuses on the maximum strain values obtained from the stirrups within the same cross-section. The strain measurement points for the longitudinal bars are located at the center of the bottom longitudinal bars, labeled as point A. The arrangement of these reinforcement strain gauges is illustrated in Fig. 6.

3 Test results and discussions

3.1 Load-deflection test results

To investigate the variation patterns of mid-span deflection in ordinary RCB and UHPC reinforced beams with

Table 4 Steel material properties

Rebar grade	Diameter (mm)	Yield strength (MPa)	Ultimate strength (MPa)	Elastic modulus (GPa)
HPB300	6	375	510	210
HPB300	8	344	461	210
HPB300	10	348	470	210
HRB400	22	448	622	200

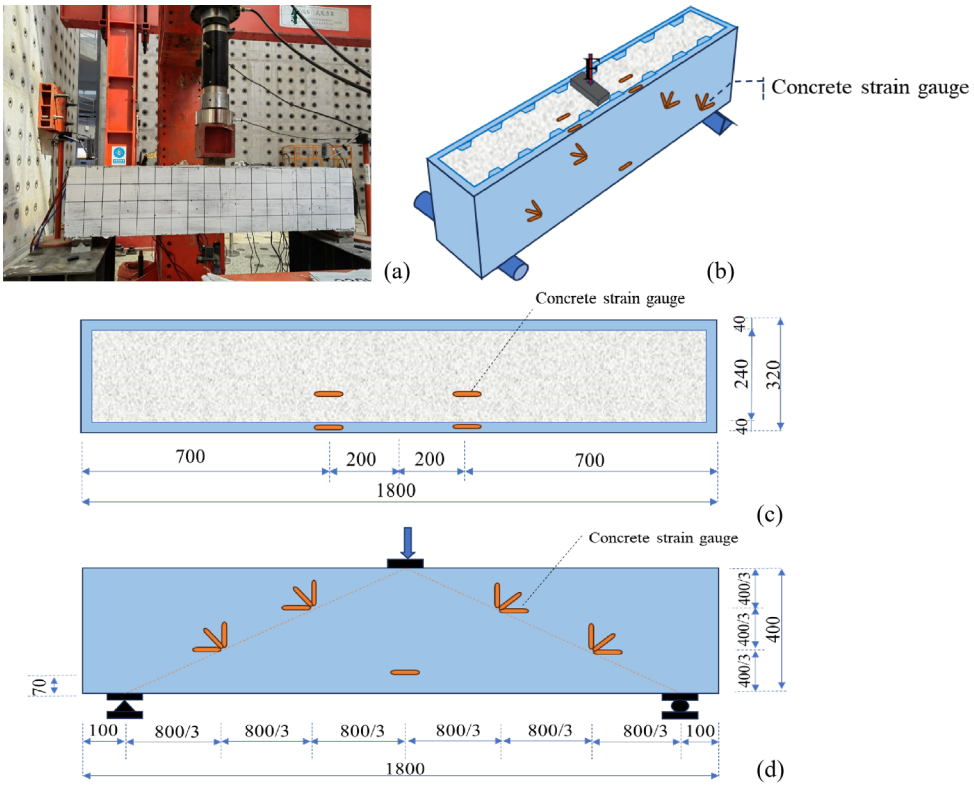

Fig. 5 Model beam loading diagram: (a) on-site test loading arrangement, (b) loading schematic diagram, (c) strain gauge layout on top surface of beam concrete, (d) strain gauge layout on side surface of beam concrete

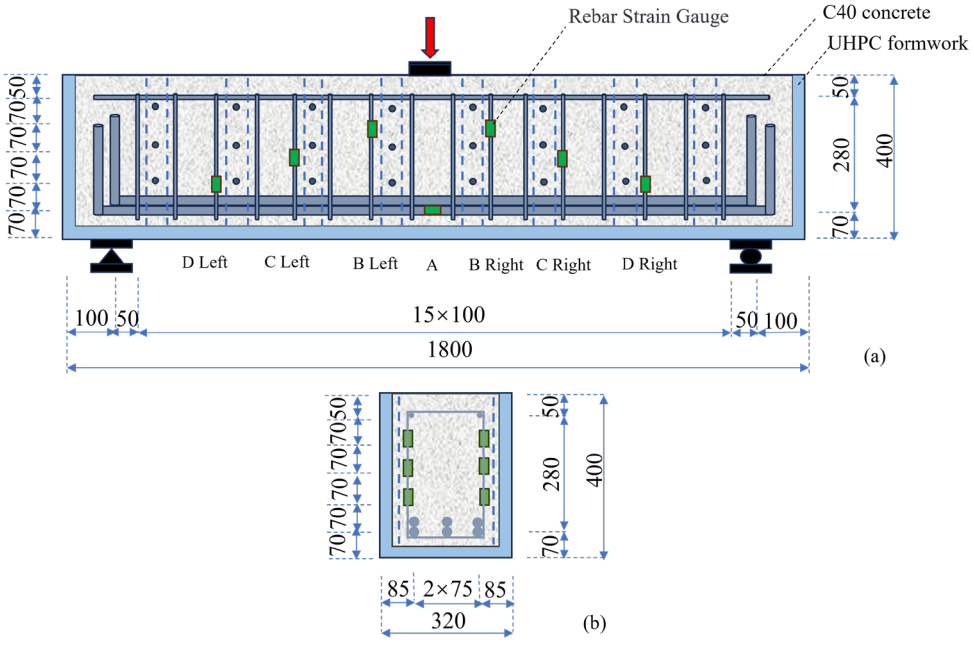

Fig. 6 Layout diagram of steel bar strain gauge: (a) front view and (b) side view

varying UHPC thicknesses, the mid-span deflection results, adjusted for support deflection, were compiled and are presented in Fig. 7. The load-mid-span deflection curve evolution can be categorized into four distinct phases. The first phase, known as the elastic phase, precedes the emergence of vertical cracks in the mid-span region of the beam. The RCB beam cracked at 80 kN, while the UR-30-D8, UR-40-D8, and UR-50-D8 beams cracked at 200 kN, 240 kN, and 220 kN, respectively. During this phase, the deflection of each model beam increased approximately

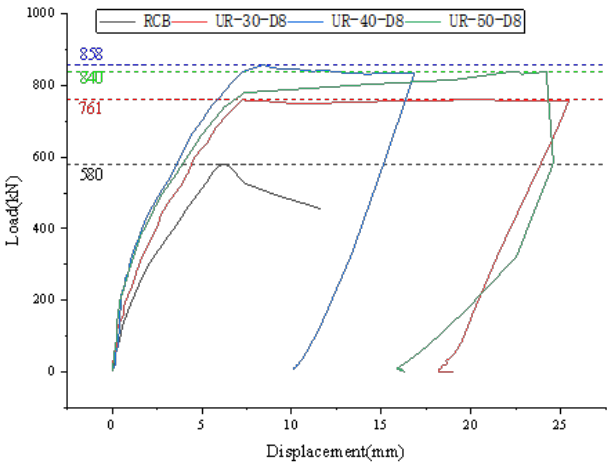

Fig. 7 Load-midspan deflection relation curve

linearly with the load, maintaining a consistent beam stiffness. The second phase marks the development of vertical cracks, which propagate from the mid-span towards both ends, leading to a degradation in beam stiffness. In the ordinary concrete RCB beam, the concrete loses its tensile load-bearing capacity upon cracking at the mid-span, transferring the tensile stress at the crack to the reinforcement. For the UR composite beams with varying UHPC thicknesses, the presence of steel fibers at the crack means that the tensile force is shared between the reinforcement and the steel fibers. Consequently, the stiffness degradation in the RCB beam is more pronounced than in the UR composite beams, and the rate of deflection increase is also greater in the RCB beam. During this phase, the load-deflection relationship of the beam exhibits non-linear growth. The third phase involves the development of diagonal cracks. Once the vertical cracks cease to extend towards the beam ends, they begin to incline towards the loading points. In this phase, the strain on the stirrups of the test beams increases, and the mid-span deflection accelerates. Observations during this phase revealed that increasing the UHPC thickness from 30 mm to 40 mm significantly enhanced stiffness; however, a further increase to 50 mm resulted in a slight decrease in stiffness. The fourth and final phase is the failure phase. After reaching the peak load, the RCB beam experienced a sharp decline in load capacity accompanied by continuous increases in deflection. In contrast, the UR composite beams did not exhibit a sudden drop in load after reaching their peak; instead, the load fluctuated within a narrow range around the peak load.

To provide a clear overview of the key shear performance indicators, the cracking loads and ultimate shear capacities of all four test beams are summarized in Table 5. These values are derived from the load-deflection curves presented in Fig. 7. As shown in Table 5, the UR beams

Table 5 Summary of cracking load and ultimate shear capacity

Beam type	Cracking load (kN)	Ultimate shear capacity (kN)
RCB	80	320
UR-30-D8	200	420
UR-40-D8	240	460
UR-50-D8	220	470

exhibited significantly higher cracking loads (150–200% increase) and ultimate shear capacities (31–48% increase) compared to the conventional RCB beam. Among the UR beams, the cracking load increased with UHPC thickness up to 40 mm, while the UR-50-D8 showed a slight decrease in cracking load but the highest ultimate capacity.

3.2 Top strain of beam

To investigate the strain variation patterns in the inner NC (normal concrete) and outer UHPC of RCB beams and UR beams with varying UHPC thickness, four concrete strain gauges were installed at corresponding positions on the top surfaces of both types of beams. Fig. 8. illustrates the strain results from the top inner NC and outer UHPC for the same beam model.

As shown in Fig. 9(a), after the load reached 300 kN, a sudden change in strain was observed in both the inner and outer NC sections of the RCB beam. The development of cracks on the top surface of the RCB beam at failure, as depicted in Fig. 10(a), reveals localized crushing damage that resulted in a long longitudinal crack precisely between the inner and outer strain gauges. Additionally, vertical cracks on the side of the beam approached the top after reaching 300 kN, leading to the speculation that unloading of concrete after 300 kN caused the strain gauges to fail. In contrast, the normal concrete within the UHPC showed minimal damage except for slight crushing at the loading point, indicating that the UHPC in UR beams effectively reduces deformation in the compressed region of normal concrete.

Comparing the strains on the inner and outer sides of the UR beam top, it was found that for the UR-30-D8, UR-40-D8, and UR-50-D8 beams, the outer UHPC strain exceeded the inner NC strain. This suggests that the internal normal concrete transfers most of the load through bolts to the higher-strength UHPC, thereby achieving better load sharing between the UHPC and normal concrete. When the experimental loads reached the ultimate loads for each beam, the maximum compressive strains on the outer UHPC side of the beam tops were −1808με, −1843με, and −1856με, respectively, none of which reached the ultimate compressive strain capacity of UHPC.

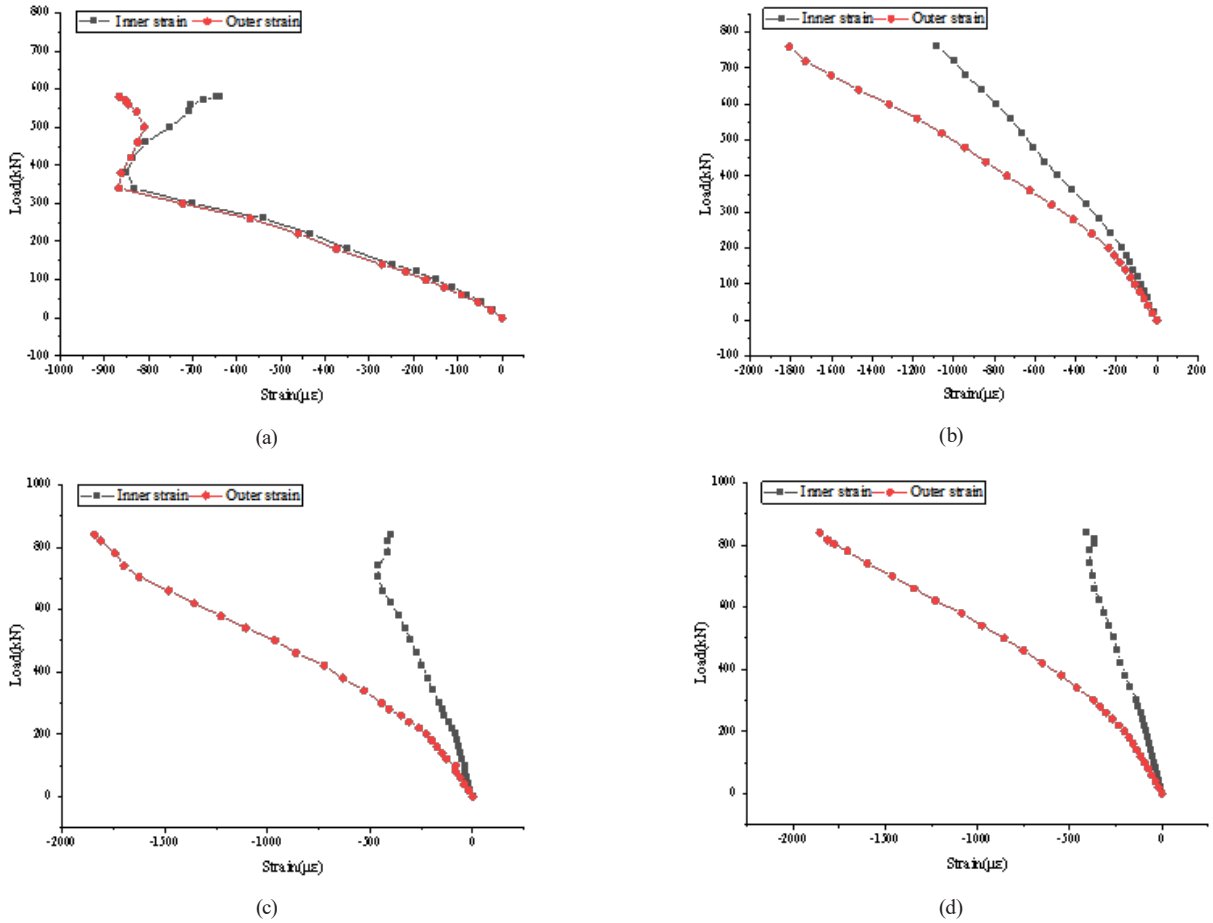

Fig. 8 Comparison of beam top strain under the same working condition: (a) RCB beam, (b) UR-30-D8 beam, (c) UR-40-D8 beam, (d) UR-50-D8 beam

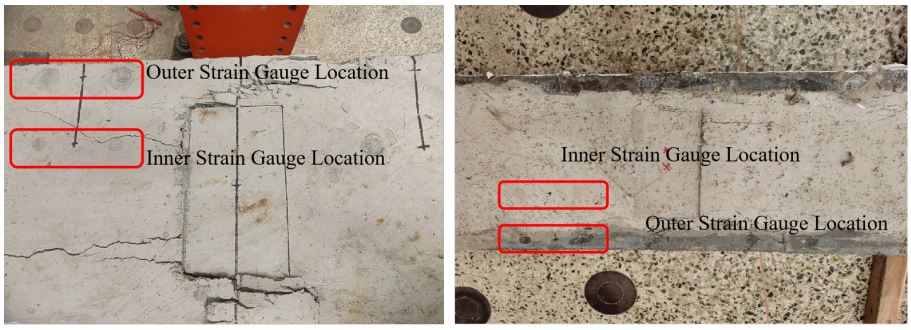

Fig. 9 Cracks on beam top surface: (a) RCB beam top surface, (b) UR-30-D8 beam top surface

As shown in Fig. 10, the figure compares the top inner NC (normal concrete) strain and outer UHPC strain for RCB beams and UR composite beams with different UHPC thicknesses. Before loading reached 300 kN, the inner and outer strains of the UR composite beams with varying UHPC thicknesses were lower than those of the RCB beams, and the compressive strain in the top concrete before cracking exhibited a nearly linear change. The top inner NC strain variation patterns for the UR-40-D8 and UR-50-D8 beams were essentially identical, with minimal differences in strain values, which were significantly lower than the top NC strain changes in the RCB beams under the same load. Under the same loading conditions, the top inner NC strain change patterns for different UHPC thickness UR beams followed this order: RCB > UR-30-D8 > UR-40-D8 > UR-50-D8. As the UHPC thickness increased, the top inner NC strain gradually decreased.

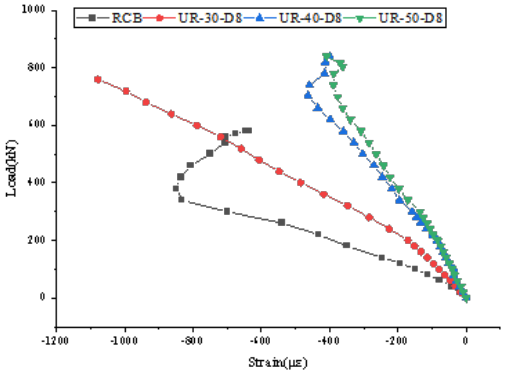

(a)

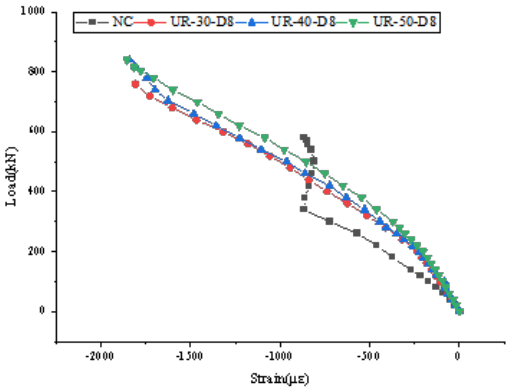

(b)

Fig. 10 Comparison of beam top strain under different working conditions. (a) The strain on the inner side of the beam's top in NC. (b) The strain on the outer side of the beam's top in UHPC.

These observations indicate that the outer UHPC can effectively reduce the deformation of the internal normal concrete. The thicker the UHPC layer, the more pronounced its effect on reducing the deformation of the compressed region of the normal concrete.

3.3 Side strain of beams

To investigate the distinct strain patterns in the side surface concrete of RCB beams and UR beams with varying UHPC thicknesses, a concrete strain gauge was installed at the bottom of each beam's side to monitor the cracking load. Additionally, right-angle strain rosettes were used to study the principal strain variation in the NC (normal concrete) and UHPC on the beam sides. Fig. 11 illustrates the strain variation patterns at the bottom of the side surfaces for UR beams with different UHPC thicknesses. From the figure, it can be observed that: The load at which strain abruptly changes for the RCB, UR-30-D8, UR-40-D8, and UR-50-D8 beams is consistent with their respective cracking loads, showing an approximately linear relationship. Due to the location of vertical cracks near the strain

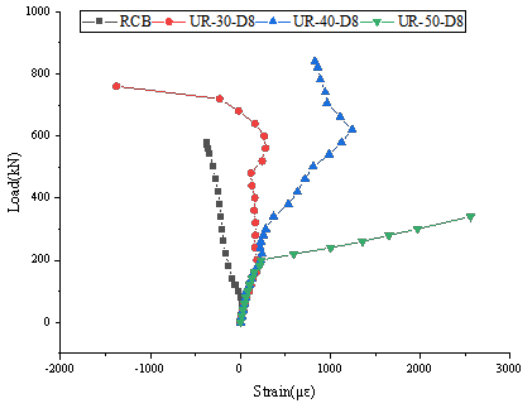

Fig. 11 The strain comparison of concrete at the bottom of the beam side

measurement points at mid-span, the concrete strain gauges either fail or show a sharp increase after the beams crack.

As shown in Fig. 12, before the appearance of diagonal cracks, the principal strain increases gradually, with relatively small values. After the load reaches 300 kN:

For the RCB beam, diagonal cracks extend from the loading point towards the support at approximately a 45° angle, reaching the bottom of the beam, causing the strain gauge to fail. For UR composite beams with different UHPC thicknesses, vertical cracks primarily develop after 400 kN, starting from the bottom and tilting towards the mid-span loading point. This results in a gradual increase in the principal strain on the beam sides, especially near the supports. Once a crack passes through a particular strain gauge, it leads to gauge failure, which affects the calculated principal strain values derived from the strain rosette measurements.

3.4 Strain of NC inside the beam

To investigate the strain variation patterns in the internal normal concrete (NC) of RCB beams and UR beams with different UHPC thicknesses, a vibrating-wire concrete strain gauge was installed beneath the bottom longitudinal reinforcement to measure the strain in the bottom NC. Fig. 13 illustrates the strain variation patterns of the embedded concrete gauges in UR beams with varying UHPC thicknesses. From the figure, it can be observed that for the RCB, UR-30-D8, UR-40-D8, and UR-50-D8 beams, the relationship between strain and load is approximately linear before cracking occurs. After cracking, the strain increases rapidly with increasing load.

As shown in Fig. 14, the main crack positions in the UR-30-D8 and UR-50-D8 beams are located between the strain gauges, leading to significant deformation in the mid-span region of the normal concrete. Based on these

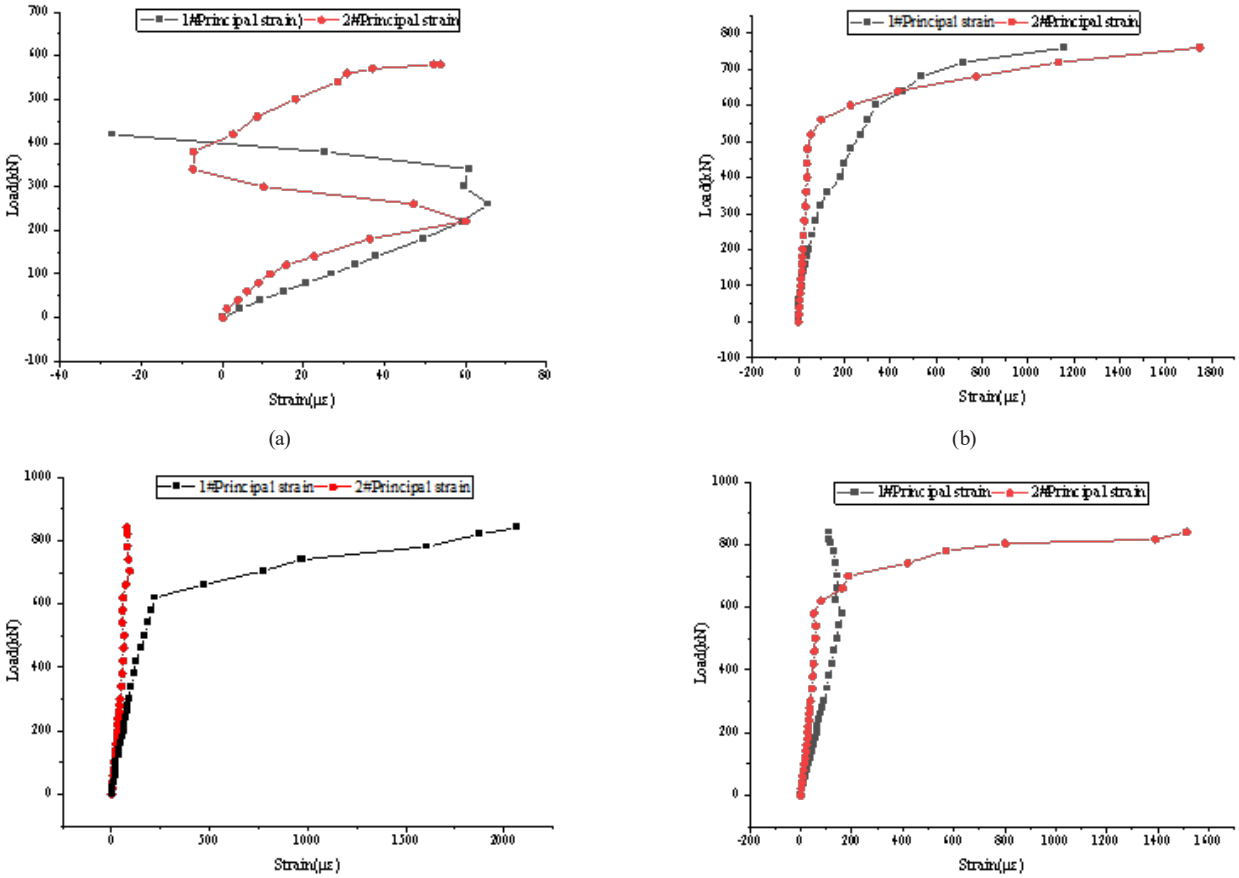

Fig. 12 Load-main strain curves of beams under various working conditions: (a) RCB beam, (b) UR-30-D8 beam, (c) UR-40-D8 beam, (d) UR-50-D8 beam

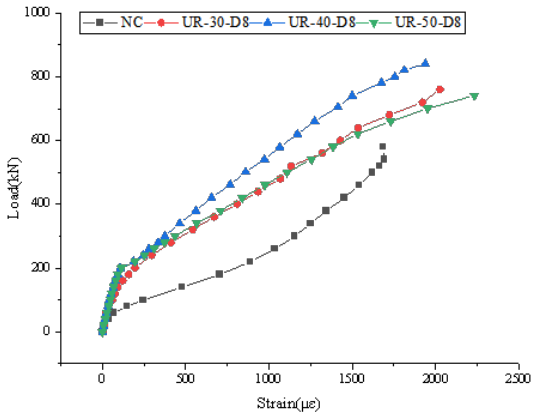

Fig. 13 Load - built-in concrete gauge strain curve

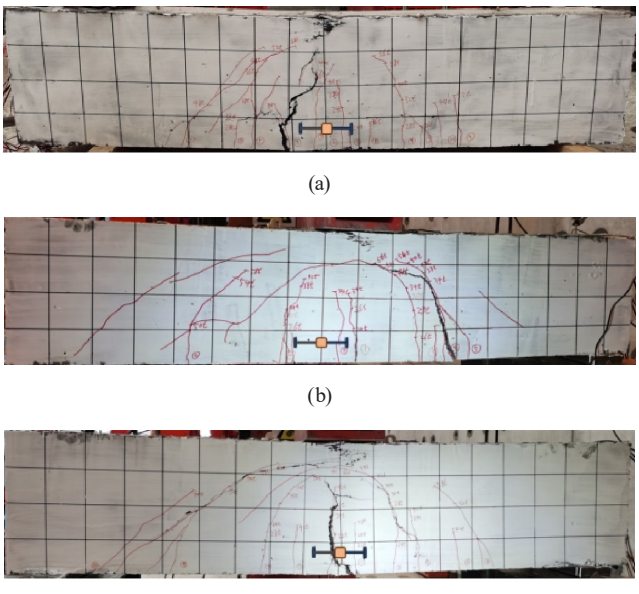

Fig. 14 The position of the built-in concrete gauge and the main crack position: (a) UR-30-D8 beam, (b) UR-40-D8 beam, (c) UR-50-D8 beam

observations, it is evident that using ribbed UHPC can effectively reduce the deformation of the internal tensile zone of normal concrete.

3.5 Strain in stirrups

This study also investigates the strain variation patterns of stirrups within the same cross-section of RCB beams and UR composite beams with different UHPC thicknesses. As shown in Fig. 15, the stirrup strain in the model beams is closely related to the development of diagonal cracks. During the initial vertical crack development stage, the stirrup strain values in both RCB beams and UR composite

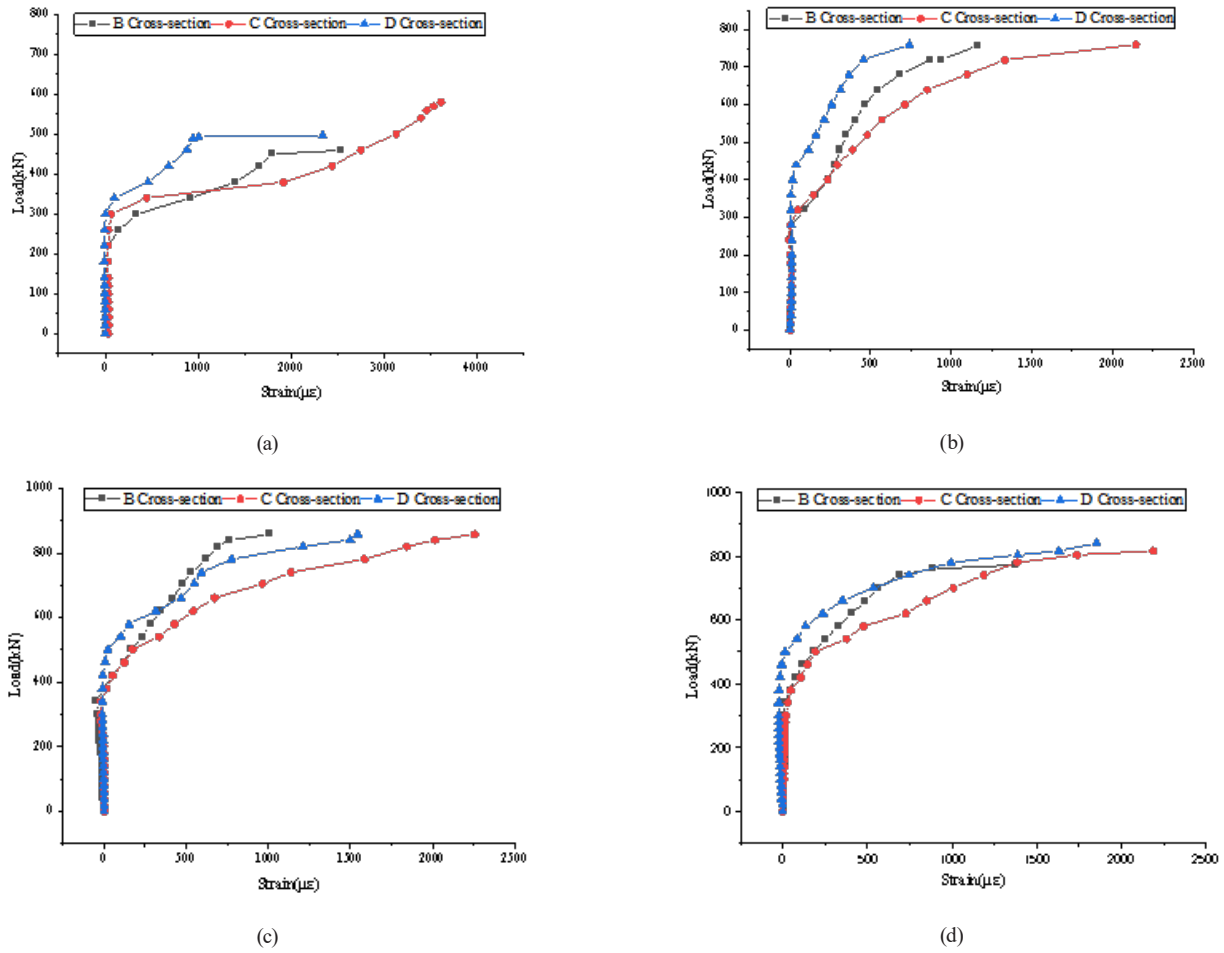

Fig. 15 Stirrup strain of each section under the same working condition: (a) RCB beam, (b) UR-30-D8 beam, (c) UR-40-D8 beam, (d) UR-50-D8 beam

beams remain relatively unchanged. As the load continues to increase, the vertical cracks extend laterally along the beam and tilt towards the loading point, leading to an increase in stirrup strain across various sections. Due to the presence of steel fibers in UHPC, the material can still bear some tensile stress after cracking, resulting in a slower increase in stirrup strain. When approaching the peak load, the width of the diagonal cracks continuously increases, and the steel fibers gradually pull out. Consequently, most of the shear force is transferred to the stirrups, causing a rapid increase in stirrup strain. It was observed that the stirrup strain is highest in the C section area.

In order to visually analyze the strain of hoop reinforcement and the development of diagonal cracks in different model beams, the position of hoop reinforcement strain gauges is marked in the beam failure diagram, as shown in Fig. 16.

To compare the stirrup strain in the same cross-section of RCB beams and UR composite beams with varying UHPC thicknesses, as shown in Fig. 17, the following observations can be made for each critical section (B, C, D):

In B Section Stirrup Strain, at a load of approximately 200 kN, the stirrups exhibit a sudden change and rapidly yield. UR-30-D8 Beam: A sudden change occurs at around 240 kN. UR-40-D8 and UR-50-D8 Beams: A sudden change occurs at approximately 300kN. Before reaching peak load, the stirrups in the B section of UR beams do not yield. Under the same loading conditions, the magnitude of stirrup strain follows this order: RCB > UR-30-D8 > UR-50-D8 > UR-40-D8.

In C Section Stirrup Strain, RCB Beam: A sudden change and rapid yielding occur at about 240 kN. UR-30-D8 Beam: A sudden change occurs at around 280 kN. UR-40-D8 and UR-50-D8 Beams: A sudden change occurs at approximately 380 kN.

The magnitude of stirrup strain and the load-induced sudden changes in the C section follow this pattern: RCB > UR-30-D8 > UR-40-D8 ≈ UR-50-D8.

In D Section Stirrup Strain, RCB Beam: A sudden change and rapid yielding occur at about 300kN. UR-30-D8 Beam: A sudden change occurs at around 400 kN.

UR-40-D8 and UR-50-D8 Beams: A sudden change occurs at approximately 500kN.

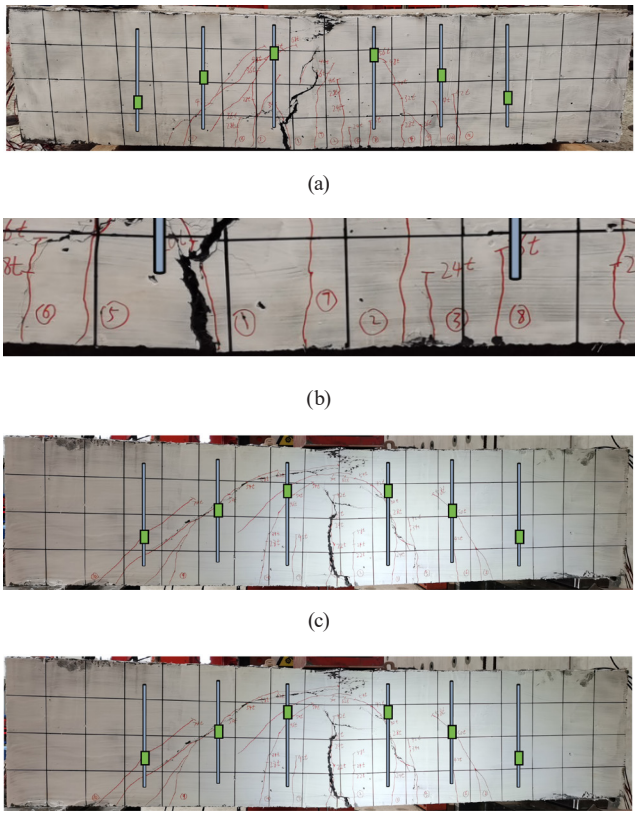

(a)

(b)

(c)

(d)

Fig. 16 The location of stirrups in the test: (a) RCB beam, (b) UR-30-D8 beam, (c) UR-40-D8 beam, (d) UR-50-D8 beam

For the D section of the UR-30-D8 beam, the stirrup strain is relatively small even at peak load. As shown in Fig. 17(b), no diagonal cracks develop in the stirrup region of the D section, indicating that increasing UHPC thickness can better utilize the performance of stirrups in each section.

Through the comparative analysis of stirrup strain in various sections, it was found that the stirrup strain in RCB beams is consistently higher across all sections. This phenomenon is closely related to the development of diagonal cracks in RCB beams. After loading reaches 300 kN, diagonal cracks in RCB beams extend from the top center at a 45° angle to the bottom of the beam, causing a sharp increase in stirrup strain. As the load continues to increase, the width of these main diagonal cracks also increases. In contrast, for UR composite beams with different UHPC thicknesses, vertical cracks at the bottom only begin to tilt towards the mid-span loading point after approximately 400 kN, and these cracks remain relatively narrow. Based on these reasons, the stirrup strain in RCB beams is significantly higher than in UR composite beams.

3.6 Crack morphology and failure analysis

As shown in Fig. 18, the curves represent the load versus maximum crack width variation for RCB beams and

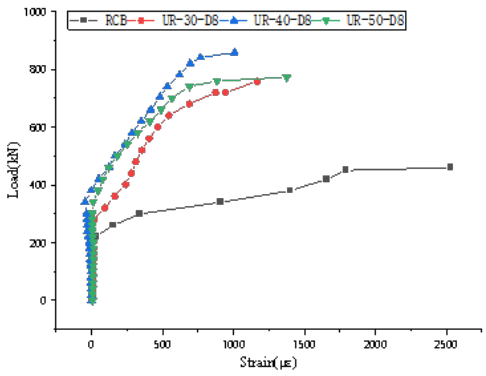

(a)

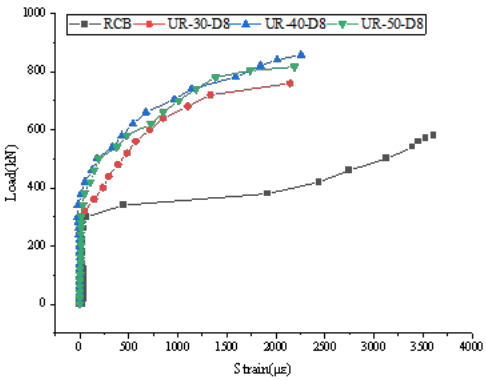

(b)

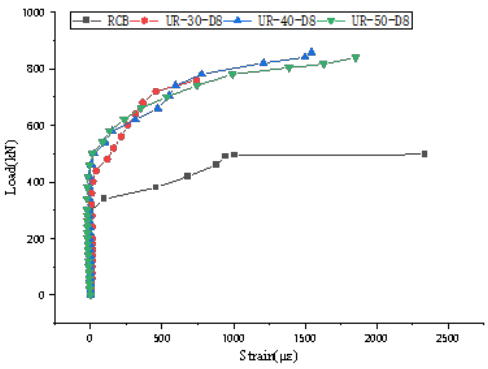

(c)

Fig. 17 Stirrup strain comparison of the same section: (a) Section B, (b) Section C, (c) Section D

UR composite beams with varying UHPC thicknesses. For comparative analysis, the crack widths are analyzed when they have developed to approximately 1 mm under different loading conditions. Under the same load conditions, the main crack width of the RCB beam increases most rapidly. After loading reaches 300 kN, the main crack width grows significantly. Observations during the crack development indicate that noticeable diagonal cracks form in the RCB beam after 300 kN. In the early stages of loading, the main crack width in UR beams gradually increases as the load increments, without any sudden increases in crack width. This behavior is attributed to the bridging effect of steel fibers within the UHPC. Cracks in

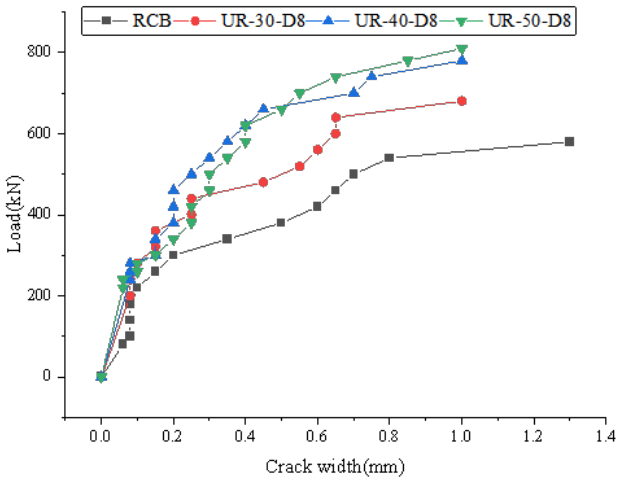

Fig. 18 Load-maximum crack width curve

UHPC tend to be multiple fine cracks rather than a single large crack. After concrete cracking, the tensile stresses originally borne entirely by the reinforcement are shared between the steel fibers in the UHPC and the reinforcement, thereby reducing the tensile stress on the reinforcement and consequently minimizing the crack width. The presence of UHPC significantly mitigates the cracking effect in composite beams, reducing both the initial crack width and the rate at which crack widths increase post-cracking. Compared to RCB beams, the development of crack widths in UR beams is notably slower after the initial cracking occurs. This indicates that UHPC enhances the structural integrity and durability of composite beams by effectively managing crack propagation.

For UR composite beams with different UHPC thicknesses, the number of visible cracks observed were as follows: UR-30-D8 beams developed 12 cracks, UR-40-D8 beams developed 11 cracks, and UR-50-D8 beams also developed 12 cracks. Compared to the conventional concrete RCB beams, which exhibited only 6 cracks, the UR beams showed a significantly higher number of cracks. This phenomenon is attributed to the high tensile strength and strain-hardening characteristics of UHPC. After cracking, UHPC exhibits multiple fine crack propagation rather than fewer but wider cracks, resulting in a larger number of narrower cracks.

Based on the experimental data, a preliminary quantitative assessment of the relationship between UHPC thickness and shear performance was conducted. The cracking loads for RCB, UR-30-D8, UR-40-D8, and UR-50-D8 were 80 kN, 200 kN, 240 kN, and 220 kN, respectively. The corresponding ultimate shear capacities were 320 kN, 420 kN, 460 kN, and 470 kN. These results indicate a clear increasing trend in both cracking load and ultimate capacity with UHPC thickness. On average, each 10 mm increase in UHPC thickness contributed to approximately 40–50 kN improvement in cracking load and 35–45 kN enhancement in ultimate capacity within the tested range. While these observations provide useful engineering references, it should be noted that they are based on a limited dataset (one specimen per configuration) and require further validation with more specimens to establish reliable design formulas.

3.7 Failure modes and crack patterns

The load versus maximum crack width relationship for all test beams is presented in Fig. 18. Under the same load level, the RCB beam exhibited the most rapid increase in main crack width. After loading to 300 kN, the crack width increased sharply, coinciding with the formation of significant diagonal cracks. In contrast, the UR beams showed gradual crack width development without sudden increases, attributed to the bridging effect of steel fibers in UHPC. This difference in crack propagation reflects the distinct failure mechanisms between conventional RC and UHPC-NC composite beams.

For the RCB beam, the first vertical crack appeared at 80 kN in the mid-span region (Fig. 19(a)). Between 80 kN and 300 kN, multiple vertical cracks developed and gradually inclined toward the loading point. At 300 kN to 380 kN, three distinct flexural-shear cracks formed, with two of them developing into dominant diagonal cracks at approximately 45°. Ultimately, brittle shear failure occurred at 580 kN, accompanied by crushing of concrete at the supports and a longitudinal crack approximately 30 cm in length on the top surface of the beam (Fig. 19(b)). The UR beams exhibited fundamentally

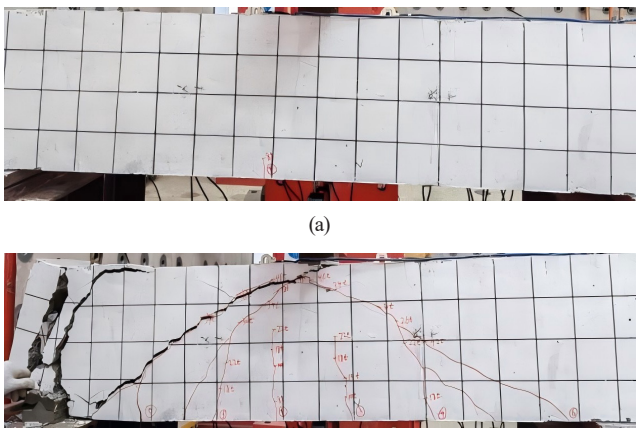

(a)

(b)

Fig. 19 Crack patterns of RCB beam (a) at cracking (80 kN) and (b) at failure (580 kN)

different crack development patterns. The UR-30-D8, UR-40-D8, and UR-50-D8 beams cracked at 200 kN (Fig. 20(a)), 240 kN (Fig. 21(a)), and 220 kN (Fig. 22(a)), respectively. These values represent a 150% to 200% increase compared to the RCB beam. As loading increased, vertical cracks developed and inclined toward the loading point. However, unlike the RCB beam, these cracks did not evolve into dominant diagonal cracks. Instead, multiple fine cracks formed. The UR-30-D8, UR-40-D8, and UR-50-D8 beams developed 12, 11, and 12 visible cracks, respectively, which is approximately double the six cracks observed in the RCB beam. Despite the larger number of cracks, their widths were significantly smaller.

At failure, all UR beams exhibited ductile flexural failure with distinctive characteristics. The UR-30-D8 beam failed at 761 kN (Fig. 20(b)), the UR-40-D8 beam at 858 kN (Fig. 21(b)), and the UR-50-D8 beam at 840 kN (Fig. 22(b)). These values represent a 31% to 48% improvement in ultimate capacity over the RCB beam (580 kN). Although the UR-50-D8 beam had a slightly lower cracking load than the UR-40-D8 beam, it achieved the highest ultimate capacity with excellent crack control, which can be attributed to the thicker UHPC layer. Failure was characterized by significant deflection, gradual load degradation after the peak, crushing of UHPC at the loading point, and audible fiber pull-out sounds. These are all indicators of ductile behavior. Notably, no interfacial slip was observed between UHPC and NC in any of the UR beams throughout loading, confirming excellent composite action.

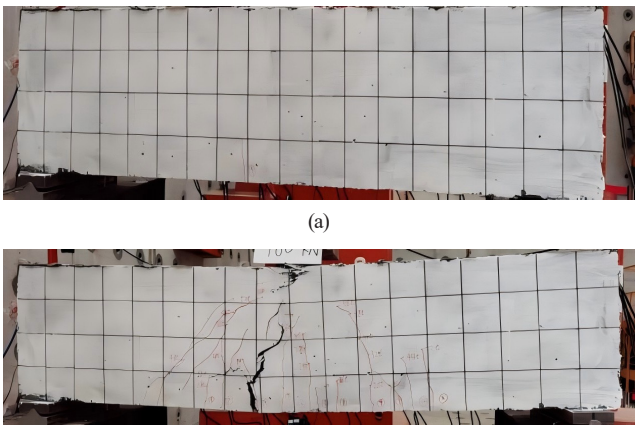

(a)

(b)

Fig. 20 Crack patterns of UR-30-D8 beam (a) at cracking (200 kN) and (b) at failure (761 kN)

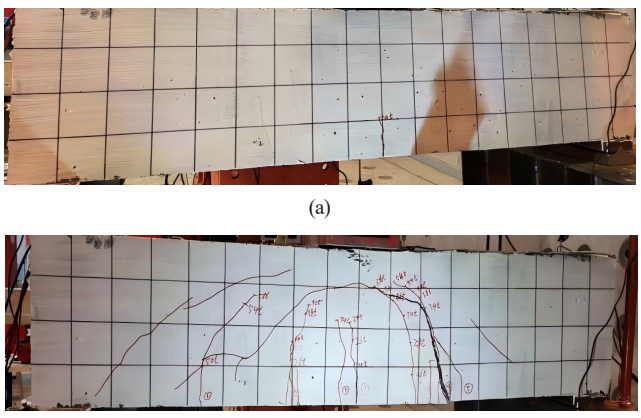

(a)

(b)

Fig. 21 Crack patterns of UR-40-D8 beam (a) at cracking (240 kN) and (b) at failure (858 kN)

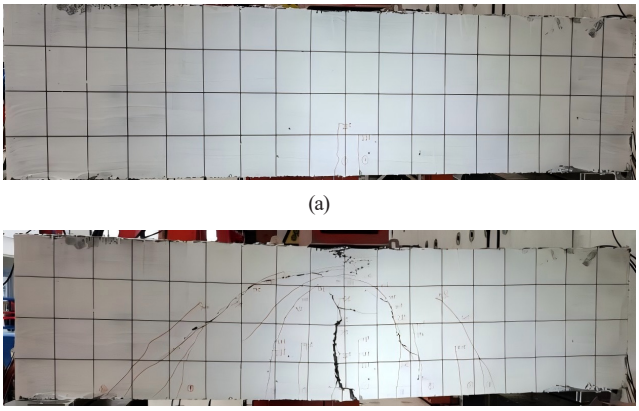

(a)

(b)

Fig. 22 Crack patterns of UR-50-D8 beam (a) at cracking (220 kN) and (b) at failure (840 kN)

4 Conclusions

This study investigated the shear behavior of UHPC-NC composite beams with ribbed UHPC thicknesses of 30 mm, 40 mm, and 50 mm through static loading tests. The main findings are summarized as follows: (1) The UR beams exhibited 150% to 200% higher cracking loads and 31% to 48% greater ultimate shear capacity compared to the conventional RCB beam. Load-deflection analysis revealed enhanced stiffness and ductility in all UR beams. (2) Strain measurements showed that the UHPC layer effectively reduced deformation in the internal normal concrete. The outer UHPC strain consistently exceeded the inner NC strain at the top surface, indicating effective load transfer through the ribbed interface. (3) Stirrup strain developed gradually in UR beams after diagonal cracking, with some sections yielding only at peak load. The steel fibers in UHPC worked synergistically with stirrups to resist shear deformation, delaying crack propagation and improving shear capacity. (4) The incorporation of UHPC transformed the brittle shear failure of conventional RC beams into ductile flexural failure. Multiple fine cracks developed in UR beams (11–12 cracks) compared to the single dominant diagonal crack in the RCB beam (6 cracks), and crack widths were significantly smaller.

A preliminary quantitative assessment suggests a positive correlation between UHPC thickness and shear performance, with each 10 mm increase in thickness contributing to approximately 35–50 kN enhancement in load capacity. However, due to experimental constraints, only one specimen was tested for each configuration. While the results show consistent trends, future studies should include replicate specimens to enable statistical analysis and incorporate vertical strain gauge arrays to track the neutral axis position for quantitative evaluation of composite action. In addition, comparative tests between ribbed and smooth interfaces are recommended to isolate the contribution of interface configuration to shear performance. A larger dataset with a wider range of UHPC thicknesses is also necessary to develop robust design formulas for engineering practice.

References

[1] Gharehbaghi, K., McManus, K., Robson, K., Eves, C., Myers, M. "Fuzzy Markov development for buried transportation bridges: review of analysis and modeling technique", International Journal of Structural Integrity, 11(2), pp. 338–353, 2020. https://doi.org/10.1108/IJSI-08-2019-0082

[2] Shi, X., Xie, N., Fortune, K., Gong, J. "Durability of steel reinforced concrete in chloride environments: An overview", Construction and Building Materials, 30, pp. 125–138, 2012. https://doi.org/10.1016/j.conbuildmat.2011.12.038

[3] Xu, F. Y., Zhang, M. J., Wang, L., Zhang, J. R. "Recent highway bridge collapses in China: review and discussion", Journal of Performance Constructed Facilities, 30(5), 04016030, 2016. https://doi.org/10.1061/(ASCE)CF.1943-5509.0000884

[4] Zhou, M., Lu, W., Song, J., Lee, G. C. "Application of ultra-high performance concrete in bridge engineering", Construction and Building Materials, 186, pp. 1256–1267, 2018. https://doi.org/10.1016/j.conbuildmat.2018.08.036

[5] Abra, O., Ben Ftima, M. "Development of a new design approach of reinforced concrete structures based on strength reduction method", Engineering Structures, 207, 110192, 2020. https://doi.org/10.1016/j.engstruct.2020.110192

[6] Lantsoght, E. O. L., van der Veen, C., de Boer, A. "Case study on aggregate interlock capacity for the shear assessment of cracked reinforced-concrete bridge cross sections", Journal of Bridge Engineering, 21(5), 04016004, 2016. https://doi.org/10.1061/(ASCE)BE.1943-5592.0000847

[7] Olajumoke, A. M., Dundu, M. "Methods for flexural strengthening of reinforced concrete elements using steel plates", In: Proceedings of the First International Conference on Construction Materials and Structures, IOS Press, 2014, pp. 1080–1085. ISBN 978-1-61499-466-4 https://doi.org/10.3233/978-1-61499-466-4-1080

[8] Nozaka, K., Shield, C. K., Hajjar, J. F. "Effective bond length of carbon-fiber-reinforced polymer strips bonded to fatigued steel bridge I-girders", Journal of Bridge Engineering, 10(2), pp. 195–205, 2005. https://doi.org/10.1061/(ASCE)1084-0702(2005)10:2(195)

[9] Jia, L., Tao, L., Hong, H., Li, Z. "Experimental test on bridge reinforcement by enlarging section-prestress method", E3S Web of Conferences, 165, 04015, 2020. https://doi.org/10.1051/e3sconf/202016504015

[10] Qiang, X., Chen, L., Jiang, X. "Experimental and theoretical study on flexural behavior of steel–concrete composite beams strengthened by CFRP plates with unbonded retrofit systems", Composite Structures, 309, 116763, 2023. https://doi.org/10.1016/j.compstruct.2023.116763

[11] Guo, S., He, H., Liu, C., Li, L. "Theoretical and experimental study on shearing capacity of concrete beams reinforced with carbon fiber truss", Composite Structures, 258, 113382, 2021. https://doi.org/10.1016/j.compstruct.2020.113382

[12] Chen, D., Sun, G., Meng, M., Jin, X., Li, Q. "Flexural performance and cost efficiency of carbon/basalt/glass hybrid FRP composite laminates", Thin-Walled Structures, 142, pp. 516–531, 2019. https://doi.org/10.1016/j.tws.2019.03.056

[13] Wang, Y. D., Yang, S., Han, M., Zhang, X. "Experimental study of section enlargement with reinforced concrete to increase shear capacity for damaged reinforced concrete beams", Applied Mechanics and Materials, 256–259, pp. 1148–1153, 2013. https://doi.org/10.4028/www.scientific.net/AMM.256-259.1148

[14] Yazici, H., Yardimci, M. Y., Aydin, S., Karabulut, A. Ş. "Mechanical properties of reactive powder concrete containing mineral admixtures under different curing regimes", Construction and Building Materials, 23(3), pp. 1223–1231, 2009. https://doi.org/10.1016/j.conbuildmat.2008.08.003

[15] Yoo, D. Y., Banthia, N. "Mechanical properties of ultra-high-performance fiber-reinforced concrete: A review", Cement and Concrete Composites, 73, pp. 267–280, 2016. https://doi.org/10.1016/j.cemconcomp.2016.08.001

[16] Yoo, D. Y., Yoon, Y. S. "A review on structural behavior, design, and application of ultra-high-performance fiber-reinforced concrete", International Journal of Concrete Structures and Materials, 10(2), pp. 125–142, 2016. https://doi.org/10.1007/s40069-016-0143-x

[17] de Larrard, F., Sedran, T. "Optimization of ultra-high-performance concrete by the use of a packing model", Cement and Concrete Research, 24(6), pp. 997–1009, 1994. https://doi.org/10.1016/0008-8846(94)90022-1

[18] Sharma, R., Jang, J. G., Bansal, P. P. "A comprehensive review on effects of mineral admixtures and fibers on engineering properties of ultra-high-performance concrete", Journal of Building Engineering, 45, 103314, 2022. https://doi.org/10.1016/j.jobe.2021.103314

[19] Amran, M., Huang, S. S., Onaizi, A. M., Makul, N., Abdelgader, H. S., Ozbakkaloglu, T. "Recent trends in ultra-high performance concrete (UHPC): Current status, challenges, and future prospects", Construction and Building Materials, 352, 129029, 2022. https://doi.org/10.1016/j.conbuildmat.2022.129029

[20] Wen, C., Zhang, P., Wang, J., Hu, S. "Influence of fibers on the mechanical properties and durability of ultra-high-performance concrete: A review", Journal of Building Engineering, 52, 104370, 2022. https://doi.org/10.1016/j.jobe.2022.104370

[21] Safdar, M., Matsumoto, T., Kakuma, K. "Flexural behavior of reinforced concrete beams repaired with ultra-high performance fiber reinforced concrete (UHPFRC)", Composite Structures, 157, pp. 448–460, 2016. https://doi.org/10.1016/j.compstruct.2016.09.010

[22] Wu, X., Kang, T. H. K., Lin, Y., Kim, J. "Shear strength of reinforced concrete beams with precast High-Performance Fiber-Reinforced Cementitious Composite permanent form", Composite Structures, 200, pp. 829–838, 2018. https://doi.org/10.1016/j.compstruct.2018.06.007

[23] Al-Madani, M. K., Al-Osta, M. A., Ahmad, S. "Interfacial bond behavior between ultra high performance concrete and normal concrete substrates", Construction and Building Materials, 320, 126229, 2022. https://doi.org/10.1016/j.conbuildmat.2021.126229

[24] Wang, Y., Qiao, P., Sun, J. "Influence of surface treatments and test methods on tensile strength of UHPC-NC interface bond", Construction and Building Materials, 456, 139051, 2024. https://doi.org/10.1016/j.conbuildmat.2024.139051

[25] Li, M., Yang, H., Huang, Y. "Interface bonding performance and mechanical properties of UHPC-NC composites", Construction and Building Materials, 502, 144312, 2025. https://doi.org/10.1016/j.conbuildmat.2025.144312

[26] Li, J., Wu, Z., Shi, C., Yuan, Q., Zhang, Z. "Durability of ultra-high performance concrete – A review", Construction and Building Materials, 255, 119296, 2020. https://doi.org/10.1016/j.conbuildmat.2020.119296

[27] Wang, X., Cheng, C., Wang, S., Lu, Z., Wang, H. "Study on the flexural behaviour of the concrete filled square steel tube beam with the basic magnesium sulfate cement-based composite shell system", Construction and Building Materials, 424, 135968, 2024. https://doi.org/10.1016/j.conbuildmat.2024.135968

[28] Huang, J., Wang, P., Shi, Q., Liu, X., Ma, H. "Flexural behavior and numerical simulation of reinforced concrete beams with a UHPC stay-in-place formwork", Structures, 69, 107254, 2024. https://doi.org/10.1016/j.istruc.2024.107254

[29] Zhang, P., Xu, F., Liu, Y., Zhao, T., Liu, J. "Shear behaviour of composite beams with permanent UHPC formwork and high-strength steel rebar", Construction and Building Materials, 352, 128951, 2022. https://doi.org/10.1016/j.conbuildmat.2022.128951

[30] Lu, W. L., Peng, W. Q., Zhu, L., Shi, J. J., Gao, D. Y. "Study on mechanical behavior of steel-UHPC-NC composite beams under negative bending moment", Case Studies in Construction Materials, 17, e01593, 2022. https://doi.org/10.1016/j.cscm.2022.e01593

[31] Li, L., Tang, J., Ye, M., Jiang, H., Zhang, Y. "Experimental study on the structural performance of a novel composite bent cap with a partially precast UHPC-steel composite shell", Composite Structures, 347, 118466, 2024. https://doi.org/10.1016/j.compstruct.2024.118466

[32] Long, J., Xiong, Y., Fu, H., Tian, L. "Flexural performance of UHPC-NC composite beams under different interface treatments: experimental, numerical analysis, and design assessment", Journal of Building Engineering, 111, 113566, 2025. https://doi.org/10.1016/j.jobe.2025.113566

[33] Zhang, Y., Yang, Z., Zhang, J. "Flexural behaviour and cost effectiveness of layered UHPC-NC composite beams", Engineering Structures, 273, 115060, 2022. https://doi.org/10.1016/j.engstruct.2022.115060

[34] Zhao, L., Luo, Q. "Evaluating bonding strength in UHPC-NC composite: A comprehensive review of direct and indirect characterization methods", Construction and Building Materials, 443, 137701, 2024. https://doi.org/10.1016/j.conbuildmat.2024.137701